Magnetic field dependence of exciton linewidth in quantum wells made of semimagnetic semiconductors: comparison of theory and experiment

2006 J. Phys.: Condens. Matter 18 7401

(http://iopscience.iop.org/0953-8984/18/31/032)

INSTITUTE OF PHYSICS PUBLISHING JOURNAL OF PHYSICS: CONDENSED MATTER

J. Phys.: Condens. Matter **18** (2006) 7401–7412 doi:10.1088/0953-8984/18/31/032

Magnetic field dependence of exciton linewidth in quantum wells made of semimagnetic semiconductors: comparison of theory and experiment

A V Komarov[1], V I Sugakov[2,4], G V Vertsimakha[2], W Zaleszczyk[3], G Karczewski[3] and T Wojtowicz[3]

[1] Institute of Physics, NASU, Prospect Nauki 46, 03028, Kiev, Ukraine
[2] Institute for Nuclear Research, NASU, Prospect Nauki 47, 03680, Kiev, Ukraine
[3] Institute of Physics, PAS, Aleja Lotników 32/46, 02-668 Warsaw, Poland

E-mail: sugakov@kinr.kiev.ua

Received 6 June 2006, in final form 28 June 2006
Published 21 July 2006
Online at stacks.iop.org/JPhysCM/18/7401

Abstract

This paper presents the result of theoretical and experimental studies of the magnetic field dependence of the exciton linewidth in $Cd_{1-y}Mg_yTe/Cd_{1-x}Mn_xTe/Cd_{1-y}Mg_yTe$ quantum wells. The reflection spectra from the structures with various values of x were measured at $T = 2$ K in magnetic fields up to 3.5 T applied parallel to the structure's growth axis. In the theoretical studies, the fluctuations of both concentration and spin projection of magnetic ions have been considered as the main reasons for the exciton line broadening. It is shown that the experimentally observed broadening of the σ^- exciton line and the narrowing of the σ^+ exciton line with increasing magnetic field are in good agreement with theoretical calculations.

1. Introduction

Bandwidth is an important parameter of optical spectra. It contains information about microscopic processes in a system and is a determining factor of its applicability in optical devices. Therefore, an analysis of the broadening of the exciton lines in quantum wells (QWs) has been a subject of a number of investigations [1–9]. The reasons for the exciton line broadening in a quantum well may be numerous: fluctuations of well thickness, interface roughness, macroscopic inhomogeneities of various kinds, and so on. These deviations from the perfect structure lead to fluctuations of the exciton band bottom and to the appearance of localized states for excitons, resulting in inhomogeneous line broadening. As the nature of the broadening of this kind is technological, a proper description of its effects requires additional fitting parameters, magnitudes of which depend on the particular technology used for

[4] Author to whom any correspondence should be addressed.

the sample preparation. In semiconductor alloys, there also exists a mechanism of broadening caused by a microscopic compositional disorder. Magnetic ions are unevenly distributed across the crystal lattice and have randomly oriented spins. This creates a potential for electrons and holes that is rapidly oscillating in space. In earlier theoretical papers [10, 11], the authors studied exciton line broadening caused by exciton scattering on component variations and fluctuations of the magnetic ion spin projection in dilute magnetic semiconductor (DMS) based quantum well structures. The fluctuations of composition and spin orientation are always present in dilute magnetic semiconductor alloys and determine the homogeneous line broadening. They can play a major role in the determination of the exciton linewidth even in the optical spectra of high-quality samples. This role can be studied without uncertainties related to the unknown values of parameters describing defects of a technological nature. Qualitatively, the mechanism of the bandwidth broadening can be explained by the disorder-induced mixing of the exciton state with a zero in-plane wavevector $\boldsymbol{k} = 0$ and the states with non-zero wavevectors $\boldsymbol{k} \neq 0$. As a result of this mixing, states with $\boldsymbol{k} \neq 0$ become optically allowed, thus contributing to the band broadening. The estimates have shown that the contribution of this scattering mechanism to the linewidth is quite large. It is also shown that the exciton linewidth has to depend substantially on the external magnetic field. There is an interesting peculiarity of this dependence, namely the narrowing of some of the lines in the external magnetic field. This effect has been explained by the coherent contribution of the spin-dependent and the spin-independent parts of the interaction between the exciton and the magnetic ions to the scattering processes [10, 11]. This feature creates a possibility of tuning the linewidth in dilute magnetic semiconductors by applying a magnetic field. The magnetic-field-induced narrowing of the linewidth was reported in [12] for bulk semimagnetic crystals. Narrowing of the exciton line was also observed in the exciton photoluminescence (PL) spectrum of the ZnSe/Zn(Cd, Mn)Se system [5]. In the present paper, an experimental study of the magnetic field effect on the exciton reflection linewidth in DMS QWs and a comparison with calculations performed in the framework of the proposed model are presented.

2. The studied system

The aim of our paper is the investigation of the effect of exciton scattering by magnetic ions on the widths of the exciton line in QW structures. Obviously, the effect will be greater if the magnetic ions are placed in the QW region rather than in the barriers. In the case of magnetic ions located in barrier layers, the scattering exists only due to the penetration of the carrier wavefunction into the barrier, thus being of importance only for narrow QWs. Therefore, in our studies, we have used quantum structures in which the QW region is made of $Cd_{1-x}Mn_xTe$ and the barriers are of $Cd_{1-y}Mg_yTe$. The choice of CdTe-based structures was motivated by the high optical quality of these materials and the expectation of a small nonmagnetic contribution to the exciton linewidth.

Four $Cd_{1-y}Mg_yTe/Cd_{1-x}Mn_xTe/Cd_{1-y}Mg_yTe$ QW structures with different concentration of magnetic ions in the QW region were grown at the Institute of Physics, PAS (Warsaw, Poland). We will explicitly discuss here the experimental results for structures with x equal to 0, 0.014 and 0.051 (samples A, B and D, respectively). The structures were grown by molecular beam epitaxy on (100)-oriented CdTe/GaAs hybrid substrates with 4.5 μm-thick CdTe buffer layers. Each of the structures contained three $Cd_{1-x}Mn_xTe$ QWs of thicknesses $L_w = 6$ ML, 10 ML, and 18 ML (1 ML = 3.24 Å is the interlayer spacing of the CdTe crystal). Samples A and B additionally contained 93 ML-thick $Cd_{1-x}Mn_xTe$ QW. The inner $Cd_{0.8}Mg_{0.2}Te$ barriers that separated the QWs were 300 Å thick. The samples also contained $Cd_{0.8}Mg_{0.2}Te$ 500 Å-thick cup layers and additional $Cd_{0.8}Mg_{0.2}Te$ buffer layers with a thickness of 1 μm for

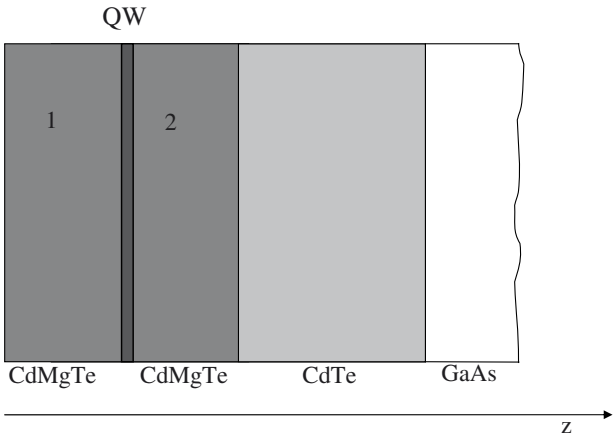

Figure 1. A schematic illustration of the heterostructure. The direction of the z-axis is opposite to the direction of the structure's growth.

samples A and D and 0.7 μm for sample B. The concentrations of Mn in the QW layers as well as the concentration of Mg in the barrier layers were determined by the position of the 1e–1hh exciton PL line, for which the energy dependence on the component content has been well studied [13, 14].

The schematic diagram of the investigated structures with only one QW is shown in figure 1.

3. Model and methods of calculations

The method of calculation of the exciton reflection spectra from a QW with semimagnetic barriers was presented in [10, 11]. In contrast to the systems investigated previously [10, 11], in this paper we consider the case of a semimagnetic QW with nonmagnetic barriers. Typical representatives of such systems are $Cd_{1-y}Mg_yTe/Cd_{1-x}Mn_xTe/Cd_{1-y}Mg_yTe$ structures. Below, we describe briefly the model that is used to calculate the frequency dependence of the light reflection coefficient for the multilayered structure.

Since the QW width is considerably smaller than the wavelength of the light, the influence of the QW on light propagation in the structure may be taken into account by the introduction of the surface conductivity caused by exciton creation [10]. So, to calculate the light reflection from a thin well, we replace the well by a surface with a surface current. The strengths of the electrical ($\boldsymbol{E}_1$, $\boldsymbol{E}_2$) and magnetic ($\boldsymbol{H}_1$, $\boldsymbol{H}_2$) fields of the light wave at each side of the QW interface are connected by the Maxwell boundary conditions in the presence of the surface current [15]:

$$\boldsymbol{E}_1(z_1) = \boldsymbol{E}_2(z_1) \tag{1}$$

$$[\boldsymbol{n}_{12}, \boldsymbol{H}_2(z_1) - \boldsymbol{H}_1(z_1)] = \frac{4\pi}{c}\boldsymbol{j}_{\text{surf}}. \tag{2}$$

Here, z_1 is the coordinate of the interface that simulates the quantum well, $\boldsymbol{j}_{\text{surf}} = \sigma^{\text{surf}}\boldsymbol{E}(z_1)$ is the density of the surface current excited by the electromagnetic wave in the quantum well, σ^{surf} is the surface conductivity, $\boldsymbol{n}_{12}$ is a unit vector normal to the surface of the quantum well and directed along the z-axis (see figure 1). In order to calculate the reflection coefficient for the structures studied, we have written the solution of the Maxwell equations for the electric

and magnetic fields in the form of the sum of the transmitted and reflected plane waves (with the exception of the terminal GaAs substrate in figure 1, where only the transmitted wave propagates) and have used the boundary conditions of (1) and (2) very well. In the present paper, only the reflection of the normally incident light is studied.

The frequency dependence of the surface current was calculated in the paper [11], where the quantum mechanical expression for the current density excited by the electromagnetic wave with frequencies close to the exciton resonance frequency of the QW was found. The current density is non-zero in the vicinity of the QW, so one can introduce the surface current by integrating the current density over the coordinate z perpendicular to the QW plane. To calculate the current density excited by light, we have used the confined 1e–1hh exciton wavefunctions, which are the solutions of the Schrödinger equation for the system considered. The corresponding Hamiltonian consists of the kinetic energy operator for the confined electrons and holes, the Coulomb interaction, and the interaction of the carriers with the magnetic ions in the QW layer and with the nonmagnetic substitutional ions in the barrier layers. The carrier–ion interactions are taken into account in the mean-field approximation, which will be discussed below. The interaction of the exciton with the magnetic ions, $H_{\rm int}$, consists of spin-dependent and spin-independent parts [11]. The spin-dependent part is caused by the exchange interaction of carriers with the unpaired electrons of the magnetic ions. The spin-independent part arises from the different values of electron densities of the substitutional atoms and the atoms of the crystal (in the case, when the contents of these atoms x and y are small, one can refer to them as 'impurity atoms' opposed to the 'crystal lattice (or host) atoms'), the deformation of the lattice in the vicinity of the substitutional atoms, and so on. The Hamiltonian of the interaction of the exciton with the substitutional ions can be written as:

$$H_{\rm int} = \sum_{\boldsymbol{n}} \frac{1}{N_0} \left\{ \left[\left(\Delta_{\rm e}^{\rm Mn} - N_0 \alpha S_{{\rm e},z} S_{\boldsymbol{n}}, z \right) \delta(\boldsymbol{r}_{\rm e} - \boldsymbol{n}) + \left(\Delta_{\rm h}^{\rm Mn} + \frac{N_0 \beta}{3} J_{{\rm h},z} S_{\boldsymbol{n},z} \right) \delta(\boldsymbol{r}_{\mathbf{h}} - \boldsymbol{n}) \right] x_{\boldsymbol{n}} + \left[\Delta_{\rm e}^{\rm Mg} \delta(\boldsymbol{r}_{\mathbf{e}} - \boldsymbol{n}) + \Delta_{\rm h}^{\rm Mg} \delta(\boldsymbol{r}_{\mathbf{h}} - \boldsymbol{n}) \right] y_{\boldsymbol{n}} \right\} \tag{3}$$

where N_0 and $\boldsymbol{n}$ are the concentration and the coordinates of the cationic lattice sites, respectively, $\Delta_{\rm e(h)}^{\rm Mn}$ and $\Delta_{\rm e(h)}^{\rm Mg}$ are the potentials of the nonmagnetic interaction of the electron (hole) with the substitutional Mn and Mg ions, respectively, $N_0\alpha$ ($N_0\beta$) is the exchange integral of the carrier–Mn^{2+} interaction for the electron (hole), $S_{{\rm e},z} = \pm 1/2$ and $J_{{\rm h},z} = \pm 3/2$ are the electron and the heavy-hole spin projections on the direction of the magnetic field (which is applied along the z-axis), $S_{\boldsymbol{n},z}$ is the spin projection of the magnetic ion, the value $x_{\boldsymbol{n}}$ describes the distribution of the impurity ions ($x_{\boldsymbol{n}} = 0$ if there is a host ion in the $\boldsymbol{n}$th lattice site, and $x_{\boldsymbol{n}} = 1$ if the site is occupied by a substitutional Mn^{2+} ion), and the value $y_{\boldsymbol{n}}$ describes the distribution of the Mg ions in a similar way.

The Hamiltonian $H_{\rm int}$ is important for subsequent considerations, so let us consider it in detail.

(1) The Hamiltonian $H_{\rm int}$ is written in the form applicable for the calculation of transition probabilities on envelope wavefunctions of electrons and holes. In microscopic approximation, we must write $\Delta V_{\rm e}^{\rm Mn}(\boldsymbol{r}_{\mathbf{e}} - \boldsymbol{n})$ instead of $\frac{1}{N_0}\Delta_{\rm e}^{\rm Mn}\delta(\boldsymbol{r}_{\mathbf{e}} - \boldsymbol{n})$, where the function $\Delta V_{\rm e}^{\rm Mn}(\boldsymbol{r} - \boldsymbol{n})$ has a sharp maximum at $\boldsymbol{r} \approx \boldsymbol{n}$. Calculations of the matrix elements of the microscopic potential $\Delta V_{\rm e}^{\rm Mn}(\boldsymbol{r}_{\mathbf{e}} - \boldsymbol{n})$ on the microscopic wavefunctions are equivalent to calculations of the matrix elements of the potential $\frac{1}{N_0}\Delta_{\rm e}^{\rm Mn}\delta(\boldsymbol{r}_{\mathbf{e}} - \boldsymbol{n})$ on the envelope wavefunctions. Here the parameter $\Delta_{\rm e}^{\rm Mn}$ is determined by the mean value of the microscopic potential on the periodic part of the Bloch wavefunction $u_{{\rm e}\boldsymbol{k}}(\boldsymbol{r}_{\mathbf{e}})$ with

a zero wavevector $\boldsymbol{k}$, i.e. $\Delta_{\mathrm{e}}^{\mathrm{Mn}} = \int u_{\mathrm{e}0}^{*}(\boldsymbol{r}_{\mathbf{e}})\Delta V_{\mathrm{e}}^{\mathrm{Mn}}(\boldsymbol{r}_{\mathbf{e}} - \boldsymbol{n})u_{\mathrm{e}0}(\boldsymbol{r}_{\mathbf{e}})\,\mathrm{d}\boldsymbol{r}_{\mathbf{e}}$ [16]. The other parameters in (3) ($\Delta_{\mathrm{h}}^{\mathrm{Mn}}$, $\Delta_{\mathrm{e}}^{\mathrm{Mg}}$, $\Delta_{\mathrm{h}}^{\mathrm{Mg}}$) are determined in a similar way. Later we will extract the magnitudes of the parameters $\Delta_{\mathrm{e(h)}}^{\mathrm{Mn(Mg)}}$ from experimental data on the depths of the quantum wells for the electrons and the holes in the absence of the magnetic field.

(2) The Hamiltonian H_{int} causes scattering of the exciton between different states and therefore leads to broadening of the exciton line. The Hamiltonian presented in the form of (3) describes processes of scattering between exciton states with different wavevectors $\boldsymbol{k}$ of the same subband only. Below, we consider the broadening of the σ^{+}- and the σ^{-}-lines of the optical transitions in these exciton subbands for a magnetic field applied perpendicularly to the QW plane, i.e. broadening of the $|-1/2, -3/2\rangle$ and $|1/2, 3/2\rangle$ 1e–1hh exciton states, respectively. The transitions between different subbands (spin-flip processes) are described by terms of the exchange interaction which are proportional to $\alpha S_{\mathrm{e}}^{\pm} S_{\boldsymbol{n}}^{\mp}$ and to $\beta J_{\mathrm{h}}^{\pm} S_{\boldsymbol{n}}^{\mp}/3$. These terms are omitted in the Hamiltonian of (3). The reasons for that are discussed in the paper [17] and are the following. The size quantization and the strain lifts the heavy–light hole degeneracy in quantum wells. The bands of heavy holes (with spin projections of $-3/2$ and $3/2$) in a quantum well split off from the bands of light holes (with spin projections $-1/2$ and $1/2$) and have lower energy. As a result, the scattering between states of heavy holes and light holes is forbidden by the energy conservation law, because the heavy holes have lower energy than the light holes. Additionally, the scattering between states with $J_z = 3/2$ and $J_z = -3/2$ is forbidden by the spin transition law. The spin-flip relaxation time related to transitions with a change of electron spin projection (between the $|-1/2, \mp 3/2\rangle$ and $|+1/2, \mp 3/2\rangle$ states) was calculated in [17]. The calculations performed in [18] showed that the probability of the spin-flip scattering in $\mathrm{Cd}_{1-x}\mathrm{Mn}_x\mathrm{Te}$ systems with a change of electron spin is much smaller than the probability of scattering between states with different $\boldsymbol{k}$ in the same subband and the same values of spin projection. This is explained by the fact that the exchange interaction of an electron with an Mn ion is weaker than the spin-independent part of the interaction. So, the main contribution to the relaxation processes comes from the scattering of excitons between states with different values of wavevector within the same subband.

Usually, in semimagnetic crystals the exciton interacts with many magnetic ions and therefore the mean-field approximation can be used, where the values of substitutional ion content $x_{\boldsymbol{n}}$ and spin orientation $S_{\boldsymbol{n},z}$ on the $\boldsymbol{n}$th site are replaced by their mean values x and $\langle S_z\rangle$. Deviations of the substitutional ion content $\delta x_{\boldsymbol{n}} = x - x_{\boldsymbol{n}}$ and spin projection $\delta S_{\boldsymbol{n},z} = S_{\boldsymbol{n},z} - \langle S_z\rangle$ from their corresponding average values (fluctuations) lead to exciton scattering. To describe this deviation, the perturbation Hamiltonian was introduced:

$$\Delta H = H_{\mathrm{int}} - H_{\mathrm{int}}^{\mathrm{meanfield}}, \tag{4}$$

where $H_{\mathrm{int}}^{\mathrm{meanfield}}$ is the Hamiltonian in the mean-field approximation. The Hamiltonian $H_{\mathrm{int}}^{\mathrm{meanfield}}$ is used to calculate the energy and the wavefunction of the exciton in the QW structure. The total Hamiltonian of the exciton in a DMS quantum well in the mean-field approximation consists of operators of the kinetic energy of the electron and the hole, the potential energy of the Coulomb interaction, the Hamiltonian of the interaction of the exciton with the magnetic ions of (3) in the mean-field approximation, and the interaction of the carriers and the magnetic ions with the magnetic field. For our calculations, we have used the popular form of the variational wavefunction of the confined exciton in the quantum well with the Hamiltonian $H_{\mathrm{int}}^{\mathrm{meanfield}}$:

$$\Psi_{\boldsymbol{k},i} = \frac{1}{\sqrt{A}} \mathrm{e}^{\mathrm{i}\boldsymbol{k}\boldsymbol{R}} \Phi_i\,(\rho, z_{\mathrm{e}}, z_{\mathrm{h}})\,|i\rangle, \tag{5}$$

$$\Phi_i\,(\rho, z_\mathrm{e}, z_\mathrm{h}) = f^\mathrm{e}_{S_z}(z_\mathrm{e})\, f^\mathrm{h}_{J_z}(z_\mathrm{h}) \sqrt{\frac{2}{\pi \lambda_i^2}}\, \mathrm{e}^{-\rho/\lambda_i}, \tag{6}$$

where $i \equiv |S_z J_z\rangle$, $\Phi_i(|\boldsymbol{\rho}_\mathrm{e} - \boldsymbol{\rho}_\mathrm{h}|, z_\mathrm{e}, z_\mathrm{h})$ is the exciton overlap wavefunction, $\boldsymbol{r}_{\mathrm{e(h)}} = (\boldsymbol{\rho}_{\mathrm{e(h)}}, z_{\mathrm{e(h)}})$ are the electron (hole) coordinates, z is the structure's growth direction; only the lowest exciton state was taken into account. The functions $f^\mathrm{e}_{S_z}(z_\mathrm{e})$ and $f^\mathrm{h}_{J_z}(z_\mathrm{h})$ in (6) are the wavefunctions of the electron and the hole of the lowest subbands in a rectangular quantum well [19], $\boldsymbol{k}$ and $\boldsymbol{R}$ are the wavevector and the position of the exciton centre of mass in the plane of the layers, λ_i is the variational parameter, and A is the layer surface area.

The perturbation ΔH, which is proportional to the linear and quadratic terms of δx_n and $\delta S_{n,z}$, describes the interaction of the exciton with the fluctuations and leads to the scattering of the exciton between states with different wavevectors [11]. According to [10], the surface conductivity reads

$$\sigma_i^\mathrm{surf}(\omega) = \mathrm{i}\frac{\omega_\mathrm{LT}\omega\varepsilon a_\mathrm{B}^3}{4} \frac{\left|\int \Phi_i\,(0, z, z)\,\mathrm{d}z\right|^2}{\omega - \omega_{0i} + \delta_i(\omega) + \mathrm{i}\,(\Gamma_0 + \Gamma_i(\omega)}, \tag{7}$$

where ω_{0i} is the bottom of the ith exciton band, ω_LT is the longitudinal–transverse splitting for the free excitons in the bulk material, a_B is the exciton Bohr radius in a bulk crystal, ε is the dielectric constant, ω is the light's frequency, ω_0 is the resonance frequency for the exciton of the considered spin subband in the QW calculated in the mean-field approximation for the exciton-substitutional ion interaction, and the fitting parameter Γ_0 describes the exciton damping due to other mechanisms of the line broadening. We shall assume that Γ_0 does not depend on either the frequency or the magnetic field. In (7), $\Gamma_i(\omega)$ and $\delta_i(\omega)$ are, respectively, the damping and the exciton resonance frequency shift caused by the exciton scattering on the magnetic ions. These values are determined by the following equation:

$$\sum_{\boldsymbol{k}} \frac{\left\langle \left|\Delta H_{i0,i\boldsymbol{k}}\right|^2 \right\rangle}{\hbar\omega_{0i} + \frac{\hbar^2 k^2}{2M} - \hbar\omega - \delta_i(\omega) - \mathrm{i}\Gamma_i(\omega)} = \delta_i(\omega) + \mathrm{i}\Gamma_i(\omega) \tag{8}$$

where $\Delta H_{i0,i\boldsymbol{k}}$ is the matrix element of the perturbation ΔH of (4), which connects the zero wavevector state of the exciton with some other $\boldsymbol{k}$-vector exciton state in the ith exciton band. This matrix element is calculated on the exciton wavefunctions obtained in the mean-field approximation. The brackets $\langle f \rangle$ denote averaging of the value of f over the random distribution of the substitutional ion concentration and spin orientation. The averaging procedure is described in detail in [11]. The average value of $\langle|\Delta H_{i0,i\boldsymbol{k}}|^2\rangle$ is proportional to $x(1-x)$, where x is the magnetic ion content. The values $\Gamma_i(\omega)$ and $\delta_i(\omega)$ were calculated numerically.

We have used the following parameters for the calculations: the valence band offset $\tilde{\alpha} = 0.4$, the effective masses of the electron and the heavy hole $m_\mathrm{e} = 0.096\ m_0$ and $m_\mathrm{h} = 0.5\ m_0$, where m_0 is the free electron mass, $N_0\alpha = 0.22$ eV, $N_0\beta = -0.88$ eV [14], the dielectric constant $\varepsilon = 9.7$, the band gap of CdTe $E_\mathrm{g}(\mathrm{CdTe}) = 1.606$ eV, the band gap of $\mathrm{Cd}_{1-x}\mathrm{Mn}_x\mathrm{Te}$ $E_\mathrm{g}(\mathrm{Cd}_{1-x}\mathrm{Mn}_x\mathrm{Te}) = 1.606 + 1.592x$ eV, [20], the band gap of $\mathrm{Cd}_{1-x}\mathrm{Mg}_x\mathrm{Te}$ $E_\mathrm{g}(\mathrm{Cd}_{1-x}\mathrm{Mg}_x\mathrm{Te}) = 1.606(1-x) + 3.6x - 0.3x(1-x)$ [21], $\Delta_\mathrm{e}^\mathrm{A} = (1-\tilde{\alpha})\frac{\mathrm{d}E_\mathrm{g}(\mathrm{Cd}_{1-x}\mathrm{A}_x\mathrm{Te})}{\mathrm{d}x}$ and $\Delta_\mathrm{h}^\mathrm{A} = \tilde{\alpha}\frac{\mathrm{d}E_\mathrm{g}(\mathrm{Cd}_{1-x}\mathrm{A}_x\mathrm{Te})}{\mathrm{d}x}$ (where A = Mn, Mg), and $\omega_\mathrm{LT} = 0.9$ meV. The empirical expressions given in [22] were used to calculate the magnetic-field-induced splitting of the bands with different spins.

For each of the samples, the broadening of the 1e–1hh exciton lines in the optical spectrum and the shift of the exciton resonance energy due to exciton scattering were calculated. The exciton resonance shift $\delta_i(\omega)$ amounts to several meV. As shown in the previous work [11], the sum of the contributions to the bandwidth of the magnetic ion concentration fluctuations

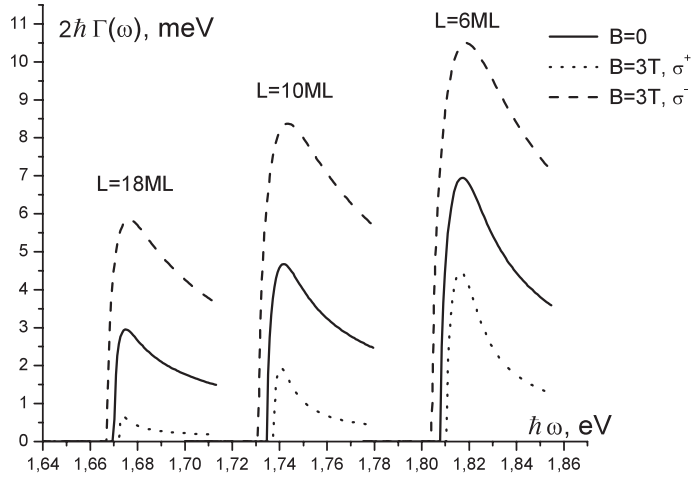

Figure 2. Damping for the σ^-- and σ^+-components of the excitonic band $\Gamma(\omega)$ as a function of the electromagnetic wave frequency for two values of the magnetic field strength in sample B (magnetic ion content $x = 0.014$; Mg ions content in the barrier is $y = 0.2$).

and spin projection fluctuations leads to the qualitatively different magnetic field dependence of the exciton linewidth for the σ^+- and σ^--bands of 1e–1hh excitons in the QW, similar to for the 'strong' σ^+- and σ^--lines of the 1s exciton spectrum in bulk semimagnetic semiconductors [12].

The dispersion of the surface conductivity of (7) has a Lorentz-like shape with frequency-dependent damping. Figure 2 shows the frequency dependence of the exciton damping $\Gamma(\omega)$ calculated with the use of the method presented for different QW thicknesses and for two values of magnetic field, $B = 0$ and 3 T.

As seen from figure 2, the scattering-induced damping parameter $\Gamma_i(\omega)$ increases with increasing B for the σ^--component and decreases for the σ^+-component. To explain this result, it should be noted that, for the spin orientation corresponding to the σ^--component, the spin-dependent part of the exciton–impurity interaction adds to the spin-independent part, while for the σ^+-component they tend to compensate each other.

For example, according to (3) the interaction of the electron of the exciton with the magnetic ion in the lattice cite $\boldsymbol{n}$ is determined by the multiplier containing the spin-dependent and the spin-independent addends, namely, $(\Delta_{\mathrm{e}}^{\mathrm{Mn}} - N_0\alpha S_{\mathrm{e},z} S_{\boldsymbol{n},z})$. These two parts are either added to each other or are subtracted from each other, depending on the electron spin projections $S_{\mathrm{e},z} = 1/2$ or $S_{\mathrm{e},z} = -1/2$. The same situation is repeated for the hole. In other words, the excitons with different spin states of the carriers interact in different ways with the magnetic ion and this leads to different probabilities of exciton scattering for different exciton spin polarizations. The difference between these probabilities depends on the strength of the magnetic field which orients the magnetic ion spins. So, there is a magnetic-field-induced suppression of the fluctuation potential and the corresponding narrowing of the σ^+-component of the exciton lines in the dilute magnetic semiconductor quantum wells.

The dependence of damping on the frequency has a maximum and drops abruptly for $\hbar\omega < \hbar\omega_{0i}$ due to the absence of the exciton states in this region of frequencies. The maximum of the damping takes place in the vicinity of $\hbar\omega \approx \hbar\omega_{0i}$, the energy at which the exciton states with a wavevector close to zero are excited ($\boldsymbol{k} \approx 0$). With an increase in the photon energy, when the value of $\hbar\omega - \hbar\omega_{0i}$ grows and the length of the exciton wave excited by the light becomes comparable to the exciton radius, the damping decreases.

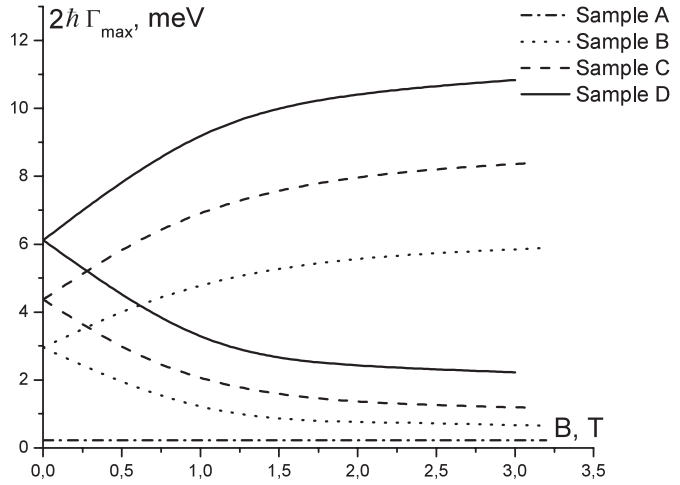

Figure 3. The magnetic field dependence of the maximum value of the exciton-scattering-induced damping $\Gamma(\omega)$ calculated for the 18 ML-wide QW for samples with different Mn contents $x = 0$, 0.014, 0.025 and 0.051 (samples A, B, C, and D, respectively).

For an illustration of the magnetic field dependence of the exciton line damping, the calculated dependence of the maximum value of $\Gamma(\omega)$ is shown in figure 3 for the $Cd_{1-x}Mn_xTe$ QWs with the same thickness (18 ML) but with different Mn content.

To calculate the light reflection coefficient for the multilayer structure used in our studies, we have employed a traditional method which takes into account the presence of the incident and reflected light waves in every layer and the boundary conditions (1) and (2) on the wells. For a detailed study of the reflection coefficient for the structure with a single QW as a function of surface conductivity, see [11].

4. Experimental results and discussion

Optical reflection spectra for the samples described in section 2 were measured at a temperature of $T = 2$ K in the Faraday geometry. A magnetic field of up to 3.5 T was produced by a superconducting solenoid and applied parallel to the growth axis of the structures.

Figure 4 displays the reflection spectra obtained for sample A in the normal incidence geometry. Both QWs and barrier layers in sample A do not contain magnetic ions and are therefore nonmagnetic. The observed long-period oscillations are caused by interference of the incident wave with waves reflected from the structure interfaces and from the substrate surface. These oscillations affect essentially the shape of the exciton lines and prevent a precise comparison of the experimental results with the theory. In samples B, C and D, which contain the magnetic ions, the magnetic field leads to a splitting of the energetic position of exciton lines, which depends on the exciton spin indexes due to the effect of the carrier–ion exchange interaction. As a result, in different magnetic fields and for different light polarizations, the exciton resonance lines are located in different regions of the Fabry–Perrot oscillating reflection curve and the studied effect can be observed for some of them more clearly. Therefore, below we concentrate on the results of the calculated and observed reflection spectra for the 1e–1hh exciton levels in the 18 ML-thick QWs. For these QWs, the exciton-related features are located on the flat part of the experimental reflection spectra. Moreover, the exciton level of this well has the lowest energy in comparison with the levels of other wells and, therefore, is subjected

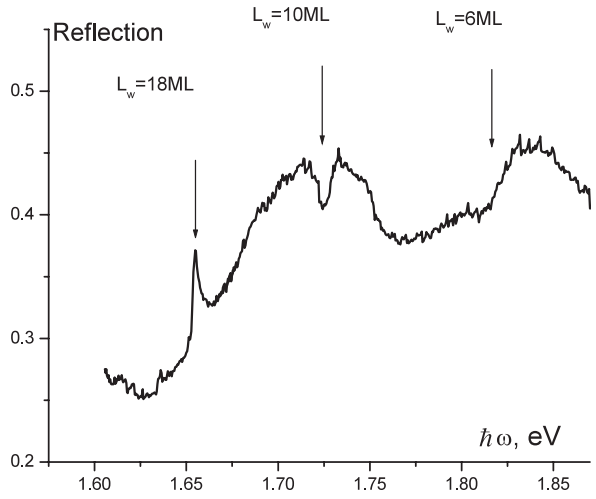

Figure 4. The normal incidence reflection spectrum taken from the nonmagnetic sample A. The arrows indicate positions of the QW heavy-hole exciton bands; L_w is the QW width.

to the influence of other wells to a small degree. In the calculations, we have taken into account the reflection from a single QW with a resonance frequency close to the investigated frequency region. This approximation is valid if the energy distance between the exciton levels of different QWs in the sample is sufficiently large. In this case, the electromagnetic field near the QW is determined first of all from the interference effects depending on the $Cd_{0.8}Mg_{0.2}Te$ cap-layer parameters as well as the $Cd_{0.8}Mg_{0.2}Te$ and CdTe buffer layers.

In our model, the exciton damping $\Gamma(\omega)$ in (7) depends on the frequency. The shape of the absorption lines calculated in the proposed model in the case of $\Gamma(\omega)_{\max} \geqslant \Gamma_0$ differs from the Lorentzian. Consequently, the shape of the reflection curve differs from the typical one, observed in the case of the Lorentzian shape of the absorption line. That is why the following method of data analysis was chosen. To characterize the bandwidth of the band with a nonstandard shape, the effective bandwidth Γ_{eff} was introduced as the distance between the positions of the maximum and the minimum of the reflectance curve. In order to compare the calculated and observed results, we have compared the effective damping Γ_{eff} obtained from the experimental reflection spectra and from the spectra calculated according to (5). The following fitting procedure was used:

(1) The fitting parameter Γ_0 (see (7)) caused by all non-Mn-related scattering mechanisms was determined to best fit the lineshapes of the measured and calculated reflection curves taken at $\boldsymbol{B} = 0$ and to obtain equal values of the effective damping (the distance between positions of the maximum and the minimum of the calculated reflectance curve) $\tilde{\Gamma}_{\text{exp}}$ and $\tilde{\Gamma}_{\text{theor}}$, respectively, for the compared spectra.
(2) The obtained fitting parameter Γ_0 was then used to calculate reflection curves for all other values of the magnetic field. To determine the bandwidth of the spectra, we have used the effective damping parameters $\tilde{\Gamma}_{\text{exp}}$ and $\tilde{\Gamma}_{\text{theor}}$ introduced in the same way as for the case $\boldsymbol{B} = 0$. Such a procedure allows one to describe the magnetic field dependence of the linewidth for the reflection line of a nonstandard shape.

The experimental results confirm a strong magnetic field dependence of the exciton linewidth in dilute magnetic heterostructures. This dependence is different for σ^+- and σ^--exciton spin

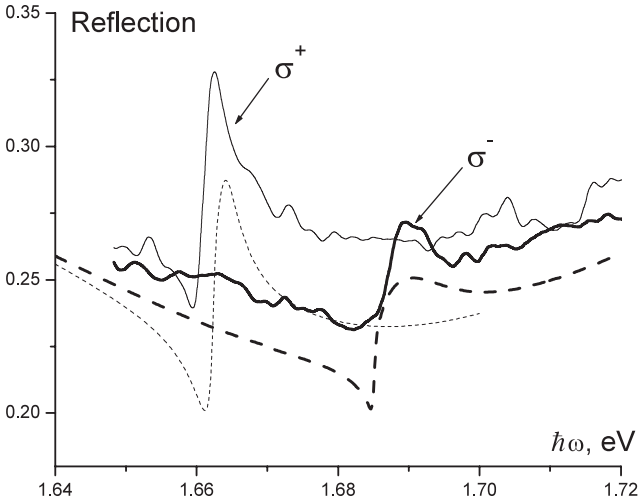

Figure 5. Normal incidence reflectance spectra for σ^+- (thin solid line) and σ^--components (thick solid line) of the exciton band of the 18 ML-wide QW with magnetic ions content $x = 0.014$. The measurements were carried out at $T = 2$ K in the magnetic field $B = 3.2$ T. Corresponding calculated curves are plotted using thin and thick dashed lines, respectively, $\hbar\Gamma_0 = 1.1$ meV).

subbands. With increasing magnetic field, the linewidth increases for the σ^--component of the exciton transition and decreases for the σ^+-component. This is seen in figure 5, where the reflection spectra taken for a 18 ML-thick QW from sample B ($x = 0.014$) are shown.

Figure 6 plots the reflection spectra for sample D with an increased magnetic ion content of 0.051 for the QW with the same width of 18 ML. The spectra are shown for the magnetic fields $B = 3$ T and $B = 0$. In this case, the exciton reflection line lies on the slope of the interference oscillation curve. The σ^+-component of the exciton reflection line in the field $B = 3$ T is much narrower than without the magnetic field. But the σ^--line is so broad that the exciton resonance vanishes.

Figure 7 shows the magnetic field dependence of the experimental and theoretical values of $\tilde{\Gamma}_{\text{theor}}$ and $\tilde{\Gamma}_{\text{exp}}$ for the 18 ML-thick QW for the samples with magnetic ion contents $x = 0.014$ (sample B) and $x = 0.051$ (sample D). Note the good qualitative and quantitative agreements between the calculated and measured results for sample B. It can be seen that the σ^+-component linewidth for sample D decreases with rising magnetic field, similar to the theoretical predictions. As the σ^--component of the exciton reflection line is not observed for sample D, only the calculated effective damping parameters are depicted here. The reason for the absence of the σ^--component may be a large width of this line, as predicted by the theory. Moreover, additional broadening may by caused by the mixing of the heavy holes and the light holes for the σ^--component with increasing magnetic field. Our calculations showed that, in sample D with an Mn concentration of 5.1% and a thickness of 18 ML, the highest state of heavy holes begins to overlap with the lowest state of light holes at magnetic fields of $B > 1$ T. In this case, other mechanisms of exciton damping related to transitions between different exciton subbands intervene, and this leads to the additional line broadening. For the σ^+ and σ^- lines of sample B (content of 1.4%) and the σ^+ line of sample D, such a crossing of the heavy hole and light hole levels does not occur for the fields considered.

The agreement of the theoretical and experimental results confirms our suggestion that the parameter Γ_0 does not depend on either the frequency or the magnetic field and that

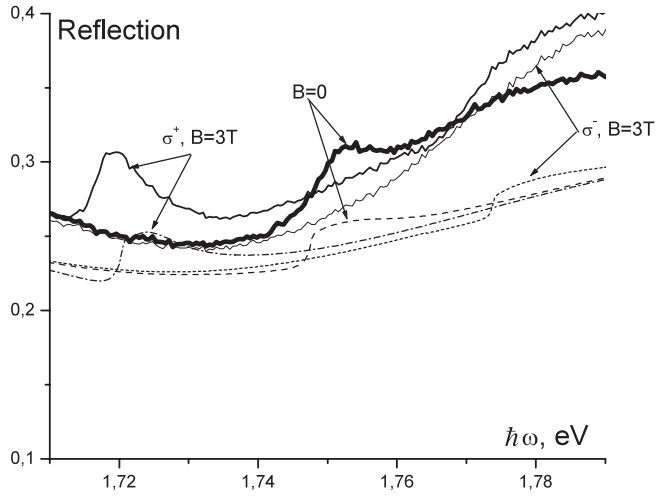

Figure 6. Normal incidence exciton reflectance spectra for the 18 ML-wide QW of sample D with magnetic ion content $x = 0.051$. Data were collected at $T = 2$ K in magnetic fields of $B = 0$ (thick solid line) and $B = 3$ T (thin solid lines). Corresponding theoretical curves are plotted by the dashed line for $B = 0$, the dash–dotted curve for the σ^+-component, and the short dashed line for the σ^--component, $\hbar\Gamma_0 = 2.7$ meV.

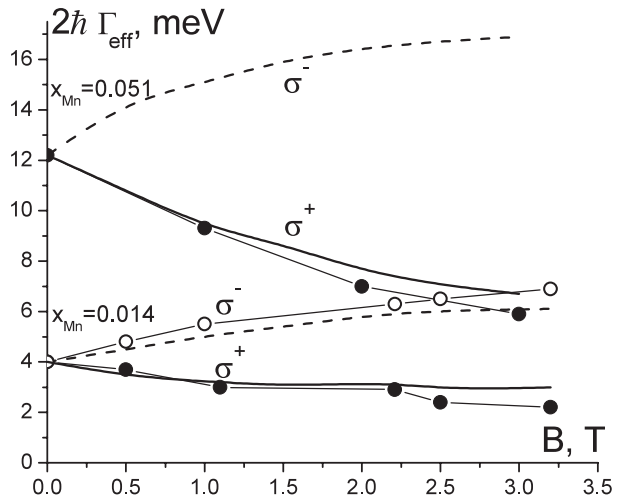

Figure 7. Magnetic field dependence of the experimental and theoretical effective bandwidths for the 18 ML-wide $Cd_{1-x}Mn_xTe$ quantum well for samples B and D. Theoretical and experimental results are shown by the thick solid curves and the black circles, respectively, in the case of the σ^+-components, and by the dashed curves and open circles in the case of the σ^- component.

the magnetic field dependence of the exciton damping is determined by the microscopic compositional disorder.

A qualitatively similar magnetic field dependence of the exciton linewidth was also observed in the reflection spectra obtained from the 10 ML-and the 6 ML-thick quantum wells in sample B, but the quantitative analysis of these results is complicated by the light interference effects. A more advanced analysis is now in progress.

5. Conclusions

Magneto-optical measurements have been performed on quantum structures containing $Cd_{1-x}Mn_xTe$ dilute magnetic semiconductor QWs with nonmagnetic $Cd_{0.8}Mg_{0.2}Te$ barriers. Excitonic reflection spectra have been studied for QWs with various concentrations of magnetic ions x. The experimental results have been compared with theoretical calculations of the exciton reflectance line shape that take into account broadening caused by the exciton scattering on the fluctuations of both the magnetic ion content and the spin projections. For the wells considered, this scattering gives the main contribution to the width of excitonic lines in the range covered by only one spin subband. In order to describe all other mechanisms of line broadening, a single magnetically independent fitting parameter Γ_0 was introduced. The theory describes correctly the experimentally observed broadening of the σ^- exciton line and the narrowing of the σ^+ exciton line with increasing magnetic field. The line narrowing is explained by the coherent summation of the spin-dependent and the spin-independent parts of the interaction between the exciton and the magnetic ions, which is a consequence of the exciton scattering within the limits of one spin subband of the 1e–1hh exciton band.

Acknowledgments

This work was supported by grant INTAS 03-51-5266 and by grant 21/09 of the Fundamental Research Foundation of Ukraine. The authors are grateful to Professor S M Ryabchenko for helpful discussions, reading and commenting on the manuscript.

References

[1] Spector H N, Lee J and Melman P 1986 *Phys. Rev.* B **34** 2554–60
[2] Baranovskii S D, Doerr U, Thomas P, Naumov A and Gebhardt W 1993 *Phys. Rev.* B **48** 17149–54
[3] Zimmermann R and Runge E 1994 *J. Lumin.* **60/61** 320–3
[4] Castella H and Wilkins J 1998 *Phys. Rev.* B **58** 16186–93
[5] Crooker S A, Rickel D G, Lyo S K, Samart N and Awschalom D D 1999 *Phys. Rev.* B **60** R2173–6
[6] Astakhov G V, Kosobukin V A, Kochereshko V P, Yakovlev D R, Ossau W, Landwehr G, Wojtowicz T, Karczewski G and Kossut J 2001 *Eur. Phys. J.* B **24** 7–13
[7] Rudin S and Reinecke T L 2002 *Phys. Status Solidi* a **190** 677–81
[8] Ramon G, Mann A and Cohen E 2003 *Phys. Rev.* B **67** 045323
[9] Ponomarev I V, Deych L I and Lisyansky A A 2005 *Phys. Rev.* B **72** 115304
[10] Sugakov V I and Vertsimakha G V 1998 *Phys. Status Solidi* b **209** 49–54
[11] Sugakov V I and Vertsimakha G V 2001 *J. Phys.: Condens. Matter* **13** 5635–44
[12] Ryabchenko S M, Semenov Yu G and Terletskii O V 1985 *Fiz. Tverd Tela* **27** 2901–8 (in Russian)
[13] Komarov A V, Ryabchenko S M, Terletskii O V, Zheru I I and Ivanchuk R D 1977 *Zh. Eksp. Teor. Fiz.* **73** 608–18 (in Russian)
[14] Gaj J A, Planel R and Fishman G 1979 *Solid State Commun.* **29** 435
[15] Jackson J 1962 *Classical Electrodynamics* (New York: Wiley)
[16] Kittel C 1963 *Quantum Theory of Solids* (New York: Wiley)
[17] Bastard G and Ferreira R 1992 *Surf. Sci.* **267** 335–41
[18] Vertsimakha G V 2005 *Ukr. Fiz. Zh.* **50** 71–7
[19] Ivchenko E L, Kavokin A V, Kochereshko V P, Posina G R and Uraltsev I N 1992 *Phys. Rev.* B **46** 7713–22
[20] Ossau W, Fiederling R, Konig B, Wojtowicz T, Kutrowski M and Kossut J 1997 *Phys. Low.-Dimen. Struct.* **11/12** 89–94
[21] Hartmann J M, Cibert J, Kany F, Mariette H, Charleux M, Alleysson P, Langer R and Feuillet G 1996 *J. Appl. Phys.* **80** 6257–65
[22] Gaj J A, Grieshaber W, Bodin-Deshayes C, Cibert J, Feuillet G, Merle d'Aubigne Y and Wasiela A 1994 *Phys. Rev.* B **50** 5512–27